

Cascaded Channel Estimation for RIS Assisted mmWave MIMO Transmissions

Yushan Liu, Shun Zhang, *Senior Member, IEEE*, Feifei Gao, *Fellow, IEEE*, Jie Tang, *Senior Member, IEEE*, and Octavia A. Dobre, *Fellow, IEEE*

Abstract

Channel estimation is challenging for the reconfigurable intelligence surface (RIS) assisted millimeter wave (mmWave) communications. Since the number of coefficients of the cascaded channels in such systems is closely dependent on the product of the number of base station antennas and the number of RIS elements, the pilot overhead would be prohibitively high. In this letter, we propose a cascaded channel estimation framework for an RIS assisted mmWave multiple-input multiple-output system, where the wideband effect on transmission model is considered. Then, we transform the wideband channel estimation into a parameter recovery problem and use a few pilot symbols to detect the channel parameters by the Newtonized orthogonal matching pursuit algorithm. Moreover, the Cramer-Rao lower bound on the channel estimation is introduced. Numerical results show the effectiveness of the proposed channel estimation scheme.

Index Terms

RIS, mmWave MIMO, wideband effect, channel estimation, NOMP, CRLB.

I. INTRODUCTION

With wide frequency bands, millimeter wave (mmWave) communications can provide unprecedented gigabits-per-second data rates and satisfy the rapidly growing transmission speed demand

Y. Liu and S. Zhang are with the State Key Laboratory of Integrated Services Networks, Xidian University, Xi'an 710071, P. R. China (Email: ysliu_97@stu.xidian.edu.cn; zhangshunsdu@xidian.edu.cn). F. Gao is with Department of Automation, Tsinghua University, State Key Lab of Intelligent Technologies and Systems, Tsinghua University, State Key for Information Science and Technology (TNList) Beijing 100084, P. R. China (Email: feifeigao@ieee.org). J. Tang is with the School of Electronic and Information Engineering, South China University of Technology, Guangzhou 510641, China (E-mail: eejtang@scut.edu.cn). O. A. Dobre is with Faculty of Engineering and Applied Science, Memorial University, St. John's NL A1C-5S7, Canada (Email: odobre@mun.ca).

of wireless communications [1]. However, radio signals in mmWave bands are sensitive to the obstacles and suffer from the severe path loss. To address this issue, many large-antenna based technologies, such as massive multiple-input multiple-output (MIMO) [2] and reconfigurable intelligent surface (RIS) assisted MIMO, have been explored. Different from radio frequency chain based MIMO systems, RIS is formed as an artificial planar structure with integrated electronic circuits, and can be programmed to manipulate an incoming electromagnetic field in a wide variety of functionalities. It consists of a large number of reconfigurable reflective elements, which can induce an adjustable independent phase shift on the incident signal [3]. Recent research results show that RIS assisted MIMO can achieve similar or even higher communication performance gains with much smaller hardware cost than massive MIMO.

Generally, RIS usually works in the passive state and has no signal processing capability [4]. Hence, channel estimation in RIS assisted wireless systems is more challenging than that in traditional systems. In [5], [6], they examined the cascaded channel estimation over the RIS aided MIMO systems. In [7], Hu *et al.* proposed a novel location information aided channel estimation method, which substantially reduced the estimation overhead. However, in the large-scale antenna systems, different antennas at the same sampling time would receive different time-domain symbols from the same physical path due to the large propagation delay of electromagnetic waves travelling across the whole antenna array, which is known as the spatial wideband effect [8]. In such case, the RIS assisted MIMO channel model in the above researches, which only considers phase difference and ignores delay difference among the transmission signals at different RIS elements and BS antennas, are not applicable anymore. Moreover, the algorithms based on such models, such as for the channel estimation and parameter recovery, need to be revised.

In this letter, we investigate the wideband channel estimation scheme for an RIS assisted mmWave MIMO system, which takes the wideband effect into consideration. The RIS assisted channels are depicted as the functions of physical parameters, including the angle of arrival/departure (AoA/AoD), the time delay and the complex gain. The phase and delay differences among the received signals at different BS antennas and RIS elements are considered. Then, the frequency response of the received signal is derived and the channel estimation is formulated as a parameter recovery problem. To achieve the acquisition of channel parameters, we resort to the Newtonized orthogonal matching pursuit (NOMP) algorithm. To make the study complete, we also derive the Cramer-Rao lower bound (CRLB). Finally, the numerical evaluations show the effectiveness of the proposed scheme.

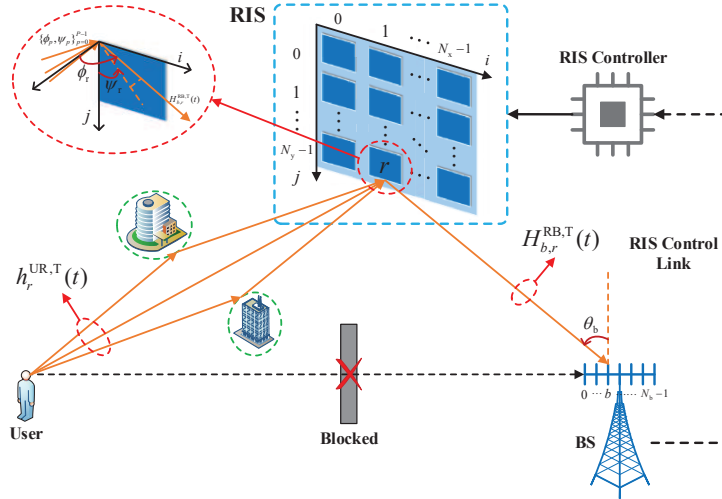


Fig. 1. An RIS assisted mmWave MIMO system.

II. WIDEBAND CHANNEL MODEL OVER RIS ASSISTED NETWORK

We consider an RIS assisted mmWave MIMO system with a single antenna user, a BS of N_b antennas and an RIS consisting of N_r passive elements, as depicted in Fig. 1. The antennas at BS form a uniform linear array (ULA), and the elements in the RIS form a uniform planar array (UPA) with N_x and N_y elements along the horizontal and vertical directions, respectively. Orthogonal frequency division multiplexing (OFDM) with N_c subcarriers is adopted for combating the multipath delay spread. Let us denote the transmission bandwidth as W , and the subcarrier spacing is $\Delta f = W/N_c$. The length of the cyclic prefix is assumed to be longer than that of the maximum multipath delay plus the maximum delay of the antenna domain.

Suppose that the multipath channel from the user to RIS consists of P incident paths. Denote $\tau_{p,r}^{\text{UR}}$ as the time delay of the p -th path from the user to the r -th element of the RIS, where $p \in \{0, \dots, P-1\}$ and $r \in \{0, \dots, N_r-1\}$. Note that $r = iN_y + j$ where $i \in \{0, \dots, N_x-1\}$ and $j \in \{0, \dots, N_y-1\}$ are the element indexes along the horizontal and vertical directions, respectively. Moreover, it can be inferred that $j = (r)_{N_y}$ and $i = (r - (r)_{N_y})/N_y$, where $j = (r)_{N_y}$ denotes the remainder of r divided by N_y . Denote ϕ_p and ψ_p as the elevation and azimuth AoAs along the p -th path at the RIS, respectively. With the RIS structure and the far-field assumption [8], $\tau_{p,r}^{\text{UR}}$ can be denoted as

$$\tau_{p,r}^{\text{UR}} = \tau_p + \frac{d \left(\frac{r - (r)_{N_y}}{N_y} \sin(\phi_p) \sin(\psi_p) + (r)_{N_y} \sin(\phi_p) \cos(\psi_p) \right)}{c}, \quad (1)$$

where d is the antenna spacing and c is the speed of light. Denote the complex path gain of the p -th path as g_p^{UR} . Then, the impulse response of the multipath channel from the user to the r -th element at the RIS can be expressed as

$$h_r^{\text{UR,T}}(t) = \sum_{p=0}^{P-1} \underbrace{g_p^{\text{UR}} e^{-j2\pi f_c \tau_p}}_{\bar{g}_p^{\text{UR}}} e^{-j2\pi \varpi_r(\phi_p, \psi_p)} \delta(t - \tau_{p,r}^{\text{UR}}), \quad (2)$$

where f_c is the carrier frequency, $\delta(\cdot)$ is the Delta function, \bar{g}_p^{UR} is the equivalent complex gain, $\varpi_r(\phi, \psi) \triangleq (d(\frac{r-(r)N_y}{N_y} \sin(\phi)\sin(\psi) + (r)N_y \sin(\phi)\cos(\psi)))/\lambda_c$ is the normalized angle at the RIS and λ_c is the carrier wavelength [8].

The direct path from the user to BS may be blocked by possible obstacles such as buildings and trees [9]. Hence, we mainly focus on the RIS assisted link. Generally, BS and RIS are considered to be located in an environment with limited local scattering, which would cause the MIMO link between BS and RIS to be a light-of-sight (LoS) [10]. Thus, we define g^{RB} as the complex path gain, θ_b as the AoA at BS, ϕ_r/ψ_r as the elevation/azimuth AoDs at RIS and $\tau_{b,r}^{\text{RB}} = bd \sin(\theta_b)/c + \varpi_r(\phi_r, \psi_r)/f_c$ as the time delay from the r -th element of the RIS to the b -th antenna of the BS, where c is the speed of light. Then, the impulse response of the LoS channel from the r -th RIS element to the b -th BS antenna can be expressed as

$$H_{b,r}^{\text{RB,T}}(t) = g^{\text{RB}} e^{-j2\pi f_c b \frac{d \sin(\theta_b)}{c}} e^{-j2\pi \varpi_r(\phi_r, \psi_r)} \delta(t - \tau_{b,r}^{\text{RB}}). \quad (3)$$

III. NOMP BASED WIDEBAND CHANNEL ESTIMATION FOR RIS ASSISTED MIMO

A. Wideband Effect on Transmission Model

By taking the Fourier transform of (2) and stacking it from RIS's different antennas into a $N_r \times 1$ vector, the frequency response between the RIS and user can be obtained as

$$\mathbf{h}^{\text{UR,F}}(f) = \sum_{p=0}^{P-1} \bar{g}_p^{\text{UR}} \mathbf{a}_R(f, \phi_p, \psi_p) e^{-j2\pi f \tau_p}, \quad (4)$$

where $\mathbf{a}_R(f, \phi, \psi) = [1, \dots, e^{-j2\pi(1+\frac{f}{f_c})\varpi_{N_r-1}(\phi, \psi)}]^T$ is the array steering vector at the RIS. By a similar mathematical manipulation on (3), the frequency response between the BS and RIS can be expressed as

$$\mathbf{H}^{\text{RB,F}}(f) = g^{\text{RB}} \mathbf{a}_B(f, \theta_b) \mathbf{a}_R^T(f, \phi_r, \psi_r), \quad (5)$$

where $\mathbf{a}_B(f, \theta) = [1, \dots, e^{-j2\pi(1+\frac{f}{f_c})(N_b-1)\frac{d \sin(\theta)}{\lambda_c}}]^T$ is the array steering vector at the BS.

Before proceeding, let us denote the RIS phase shift vector at the m -th OFDM pilot symbol as $\boldsymbol{\rho}_m \triangleq [e^{j\rho_{m,0}}, \dots, e^{j\rho_{m,N_r-1}}]^T$, where $m \in \{0, \dots, M-1\}$, M is the number of pilot symbols during channel estimation, and $\rho_{m,r} \in [0, 2\pi)$ represents the phase shift of the r -th RIS element at the m -th pilot symbol. Then, the operation of RIS can be described by the diagonal matrix $\boldsymbol{\Omega}_m = \text{diag}\{\boldsymbol{\rho}_m\} \in \mathbb{C}^{N_r \times N_r}$. Note that $\boldsymbol{\rho}_m$ is assumed to be constant during each pilot symbol. Then, the frequency response of BS's received signal at the m -th pilot symbol can be expressed as

$$\begin{aligned} \mathbf{y}_m(f) &= \sum_{p=0}^{P-1} \underbrace{g_p^{\text{RB}} \bar{g}_p^{\text{UR}}}_{g_p} \mathbf{a}_B(f, \theta_b) \mathbf{a}_R^T(f, \phi_r, \psi_r) \boldsymbol{\Omega}_m \mathbf{a}_R(f, \phi_p, \psi_p) \\ &\quad \times s_m(f) e^{-j2\pi f \tau_p} + \mathbf{v}_m(f), \end{aligned} \quad (6)$$

where g_p is defined as the cascaded complex gain, $s_m(f)$ is the frequency-domain signal from the user, and $\mathbf{v}_m(f)$ is the additive Gaussian noise with zero mean and covariance matrix $\sigma_v^2 \mathbf{I}_{N_b}$.

Assume that L out of N_c subcarriers are exclusively assigned to the user as pilots whose index set is denoted by $\mathcal{L} = \{l_0, \dots, l_{L-1}\}$. Without loss of generality, we assume that the values of all pilots are 1, i.e., $s_m(k\Delta f) = 1$, $m \in \{0, \dots, M-1\}$, $k \in \mathcal{L}$. Then, we collect the received pilot vectors $\mathbf{y}_0(k\Delta f), \dots, \mathbf{y}_{M-1}(k\Delta f)$ into an $MN_b \times 1$ vector at the k -th subcarrier as

$$\begin{aligned} \mathbf{y}(k\Delta f) &\triangleq [\mathbf{y}_0^T(k\Delta f), \dots, \mathbf{y}_{M-1}^T(k\Delta f)]^T \\ &= \sum_{p=0}^{P-1} g_p \left(\underbrace{\begin{bmatrix} \mathbf{a}_R^T(k\Delta f, \phi_r, \psi_r) \boldsymbol{\Omega}_0 \\ \vdots \\ \mathbf{a}_R^T(k\Delta f, \phi_r, \psi_r) \boldsymbol{\Omega}_{M-1} \end{bmatrix}}_{\bar{\mathbf{A}}_k(\phi_r, \psi_r) \in \mathbb{C}^{M \times N_r}} \mathbf{a}_R(k\Delta f, \phi_p, \psi_p) \right) \\ &\quad \otimes \mathbf{a}_B(k\Delta f, \theta_b) e^{-j2\pi k \Delta f \tau_p} + \mathbf{v}(k\Delta f), \quad k \in \mathcal{L}, \end{aligned} \quad (7)$$

where $\bar{\mathbf{A}}_k(\phi_r, \psi_r)$ is defined above and $\mathbf{v}(k\Delta f) = [\mathbf{v}_0^T(k\Delta f), \dots, \mathbf{v}_{M-1}^T(k\Delta f)]^T$ is the noise vector. Define $\mathbf{f}(\theta_b, \phi_r, \psi_r, \phi_p, \psi_p, \tau_p) \in \mathbb{C}^{LMN_b \times 1}$ as

$$\begin{aligned} \mathbf{f}(\theta_b, \phi_r, \psi_r, \phi_p, \psi_p, \tau_p) &= \left[\left[(\bar{\mathbf{A}}_{l_0}(\phi_r, \psi_r) \mathbf{a}_R(l_0 \Delta f, \phi_p, \psi_p)) \otimes \mathbf{a}_B(l_0 \Delta f, \theta_b) e^{-j2\pi l_0 \Delta f \tau_p} \right]^T, \dots, \right. \\ &\quad \left. \left[(\bar{\mathbf{A}}_{l_{L-1}}(\phi_r, \psi_r) \mathbf{a}_R(l_{L-1} \Delta f, \phi_p, \psi_p)) \otimes \mathbf{a}_B(l_{L-1} \Delta f, \theta_b) e^{-j2\pi l_{L-1} \Delta f \tau_p} \right]^T \right]^T. \end{aligned} \quad (8)$$

By collecting $\mathbf{y}(k\Delta f)$ at different subcarriers, we obtain

$$\begin{aligned}\mathbf{y} &\triangleq [\mathbf{y}^T(l_0\Delta f), \dots, \mathbf{y}^T(l_{L-1}\Delta f)]^T \\ &= \sum_{p=0}^{P-1} g_p \mathbf{f}(\theta_b, \phi_r, \psi_r, \phi_p, \psi_p, \tau_p) + \mathbf{v},\end{aligned}\quad (9)$$

where $\mathbf{v} \triangleq [\mathbf{v}^T(l_0\Delta f), \dots, \mathbf{v}^T(l_{L-1}\Delta f)]^T \in \mathbb{C}^{LMN_b \times 1}$ is the corresponding noise vector.

We are interested in estimating the cascaded channels at the BS from (9), which can be transformed into the problem of parameter recovery. Without loss of generality, we assume that the locations of the BS and RIS are known, which implies that the angles θ_b , ϕ_r and ψ_r can be completely determined by the geometric positions of BS and RIS. Then, $\{\theta_b, \phi_r, \psi_r\}$ are constants and can be omitted in $\bar{\mathbf{A}}_k(\phi_r, \psi_r)$ and $\mathbf{f}(\theta_b, \phi_r, \psi_r, \phi_p, \psi_p, \tau_p)$. In order to estimate the RIS assisted channel, we will resort to the NOMP algorithm to capture the parameter set $\{g_p, \phi_p, \psi_p, \tau_p\}_{p=0}^{P-1}$.

B. NOMP Algorithm

The NOMP algorithm is divided into five steps: Greedy searching, precise searching, single refinement, cyclic refinement and cascaded gain updating.

- 1) *Greedy Searching*: The over-sampled grids along the horizontal AoA, vertical AoA and delay are respectively divided with sampling rate η_ϕ , η_ψ and η_τ , where the range of actual horizontal AoA, vertical AoA and time delay are respectively $[-\pi/2, \pi/2)$, $[0, \pi/2)$ and $[0, 1/\Delta f)$. Hence, the codeword corresponding to (8) is expressed as

$$\begin{aligned}\mathbf{f}(\bar{\phi}, \bar{\psi}, \bar{\tau}) &= \left[\left[(\bar{\mathbf{A}}_{l_0} \mathbf{a}_R(l_0\Delta f, \bar{\phi}, \bar{\psi})) \otimes \mathbf{a}_B(l_0\Delta f, \theta_b) e^{-j2\pi l_0 \Delta f \bar{\tau}} \right]^T, \dots, \right. \\ &\quad \left. \left[(\bar{\mathbf{A}}_{l_{L-1}} \mathbf{a}_R(l_{L-1}\Delta f, \bar{\phi}, \bar{\psi})) \otimes \mathbf{a}_B(l_{L-1}\Delta f, \theta_b) e^{-j2\pi l_{L-1} \Delta f \bar{\tau}} \right]^T \right]^T.\end{aligned}\quad (10)$$

where $\bar{\phi} \in \{-\frac{\pi}{2}, \dots, -\frac{\pi}{2} + \frac{(\eta_\phi N_x - 1)\pi}{\eta_\phi N_x}\}$, $\bar{\psi} \in \{0, \dots, \frac{(\eta_\psi N_y - 1)\pi}{2\eta_\psi N_y}\}$ and $\bar{\tau} \in \{0, \dots, \frac{\eta_\tau N_c - 1}{\eta_\tau N_c \Delta f}\}$.

At the beginning of the i -th iteration, the residual noisy mixture \mathbf{y}_e^i is calculated by

$$\mathbf{y}_e^i = \mathbf{y} - \sum_{p=0}^{i-1} \hat{g}_p \mathbf{f}(\hat{\phi}_p, \hat{\psi}_p, \hat{\tau}_p),\quad (11)$$

where $\{\hat{g}_p, \hat{\phi}_p, \hat{\psi}_p, \hat{\tau}_p\}_{p=0}^{i-1}$ are the estimated parameters in the previous iterations. The course estimated $\hat{\phi}_i, \hat{\psi}_i, \hat{\tau}_i$ are obtained by greedily searching the grid points as

$$(\hat{\phi}_i, \hat{\psi}_i, \hat{\tau}_i) = \arg \max_{(\bar{\phi}, \bar{\psi}, \bar{\tau})} \frac{|\mathbf{f}^H(\bar{\phi}, \bar{\psi}, \bar{\tau}) \mathbf{y}_e^i|^2}{\|\mathbf{f}(\bar{\phi}, \bar{\psi}, \bar{\tau})\|^2},\quad (12)$$

where $\hat{\phi}_i$, $\hat{\psi}_i$ and $\hat{\tau}_i$ are the estimated horizontal AoA, vertical AoA and time delay of the i -th component path, respectively.

- 2) *Precise Searching*: After the simultaneously greedy searching for the three parameters, we perform a precise searching process near the results of the greedy searching step. Notice that the implementation of this process is similar to that of the greedy searching step and the details are omitted here due to space limitation. Then, the estimated parameters $\{\hat{\phi}_i, \hat{\psi}_i, \hat{\tau}_i\}$ can be obtained through a similar operation in (12). Afterwards, the coarse estimation of the cascaded gain \hat{g}_i can be obtained as

$$\hat{g}_i = \frac{\mathbf{f}^H(\hat{\phi}_i, \hat{\psi}_i, \hat{\tau}_i) \mathbf{y}_e^i}{\|\mathbf{f}(\hat{\phi}_i, \hat{\psi}_i, \hat{\tau}_i)\|^2}. \quad (13)$$

- 3) *Single Refinement*: We will resort to the extended Newton method and refine $\hat{\phi}_i$, $\hat{\psi}_i$, $\hat{\tau}_i$ and \hat{g}_i , and R_s iterations are executed in this step. The goal of the refinement step is to minimize the power of the new residual $\|\mathbf{y}_e^i - g\mathbf{f}(\phi, \psi, \tau)\|^2$ in the i -th iteration. Hence, the target is to maximize

$$\mathcal{N}(\phi, \psi, \tau) = 2\mathcal{R}\{(\mathbf{y}_e^i)^H g\mathbf{f}(\phi, \psi, \tau)\} - \|g\mathbf{f}(\phi, \psi, \tau)\|^2. \quad (14)$$

Then, the refined estimations of $\hat{\phi}_i$, $\hat{\psi}_i$ and $\hat{\tau}_i$ can be expressed as

$$\begin{bmatrix} \hat{\phi}_i \\ \hat{\psi}_i \\ \hat{\tau}_i \end{bmatrix} = \begin{bmatrix} \hat{\phi}_i \\ \hat{\psi}_i \\ \hat{\tau}_i \end{bmatrix} - \ddot{\mathcal{N}}^{-1}(\hat{g}_i, \hat{\phi}_i, \hat{\psi}_i, \hat{\tau}_i) \dot{\mathcal{N}}(\hat{g}_i, \hat{\phi}_i, \hat{\psi}_i, \hat{\tau}_i), \quad (15)$$

where $\dot{\mathcal{N}}(g, \phi, \psi, \tau) = [\frac{\partial \mathcal{N}}{\partial \phi}, \frac{\partial \mathcal{N}}{\partial \psi}, \frac{\partial \mathcal{N}}{\partial \tau}]^T$ is the first-order partial derivative vector, and

$$\ddot{\mathcal{N}}(g, \phi, \psi, \tau) = \begin{bmatrix} \frac{\partial^2 \mathcal{N}}{\partial \phi^2} & \frac{\partial^2 \mathcal{N}}{\partial \phi \partial \psi} & \frac{\partial^2 \mathcal{N}}{\partial \phi \partial \tau} \\ \frac{\partial^2 \mathcal{N}}{\partial \psi \partial \phi} & \frac{\partial^2 \mathcal{N}}{\partial \psi^2} & \frac{\partial^2 \mathcal{N}}{\partial \psi \partial \tau} \\ \frac{\partial^2 \mathcal{N}}{\partial \tau \partial \phi} & \frac{\partial^2 \mathcal{N}}{\partial \tau \partial \psi} & \frac{\partial^2 \mathcal{N}}{\partial \tau^2} \end{bmatrix} \quad (16)$$

is the second-order partial derivative matrix. According to (14), we can write the first-order partial derivatives of $\mathcal{N}(\phi, \psi, \tau)$ as $\frac{\partial \mathcal{N}}{\partial x} = 2\mathcal{R}\left\{g(\mathbf{y}_e^i - g\mathbf{f})^H \frac{\partial \mathbf{f}}{\partial x}\right\}$, where x can be ϕ , ψ and τ . The second-order partial derivative of $\mathcal{N}(\phi, \psi, \tau)$ can be calculated as $\frac{\partial^2 \mathcal{N}}{\partial x_1 \partial x_2} = 2\mathcal{R}\left\{g(\mathbf{y}_e^i - g\mathbf{f})^H \frac{\partial^2 \mathbf{f}}{\partial x_1 \partial x_2} - |g|^2 \frac{\partial \mathbf{f}^H}{\partial x_2} \frac{\partial \mathbf{f}}{\partial x_1}\right\}$, where x_1 and x_2 can be ϕ , ψ and τ . Due to the space limitation, the partial derivatives are omitted here.

By carrying out (15), $\{\hat{\phi}_i, \hat{\psi}_i, \hat{\tau}_i\}$ are refined. Then, the cascaded gain is also updated according to (13).

- 4) *Cyclic Refinement*: After the single refinement step for the parameters of the current iteration, R_c iterations of cyclically refinement are taken into consideration to further perfect the estimations $\{\hat{g}_i, \hat{\phi}_i, \hat{\psi}_i, \hat{\tau}_i\}_{p=0}^{i-1}$ of the previous iterations. Similar to the single refinement step, the extended Newton method is also utilized, and the accurate estimations $\{\hat{g}_i, \hat{\phi}_i, \hat{\psi}_i, \hat{\tau}_i\}_{p=0}^i$ can be obtained. The derivation is omitted due to space limitation.
- 5) *Cascaded Gain Updating*: Based on $\{\hat{\phi}_p, \hat{\psi}_p, \hat{\tau}_p\}_{p=0}^i$ obtained in the previous iterations, we can further update the cascaded gains through the least square algorithm as

$$[\hat{g}_0, \dots, \hat{g}_i]^T = (\mathbf{F}_i^H \mathbf{F}_i)^{-1} \mathbf{F}_i^H \mathbf{y}, \quad (17)$$

where $\mathbf{F}_i = [\mathbf{f}(\hat{\phi}_0, \hat{\psi}_0, \hat{\tau}_0), \dots, \mathbf{f}(\hat{\phi}_i, \hat{\psi}_i, \hat{\tau}_i)]$.

As the NOMP runs, the power of the residual \mathbf{y}_e^i decreases after each iteration. If the extracted parameters are accurate enough, the power of the residual is reduced to the power of the noise in the end, i.e., $\|\mathbf{y}_e^i\|^2 \approx \|\mathbf{v}\|^2$. Hence, the NOMP algorithm terminates when $|\mathbf{f}^H(\bar{\phi}, \bar{\psi}, \bar{\tau})\mathbf{y}_e^i|^2 < \epsilon$ for all possible $(\bar{\phi}, \bar{\psi}, \bar{\tau})$. The stopping criterion threshold ϵ is chosen from the false alarm rate $P_{\text{fa}} = P\{\|\mathbf{v}\|_\infty^2 > \epsilon\} = 1 - (1 - \exp(-\epsilon/\sigma_v^2))^{LMN_b}$ as $\epsilon = -\sigma_v^2 \ln(1 - (1 - P_{\text{fa}})^{1/LMN_b})$ [11].

C. Performance Analysis

To evaluate the performance of the NOMP algorithm, we derive the CRLB. Let us define the $5P \times 1$ unknown parameter vector $\boldsymbol{\xi} = [\boldsymbol{\xi}_1^T, \dots, \boldsymbol{\xi}_P^T]^T$, where $\boldsymbol{\xi}_p = [|g_p|, \angle g_p, \phi_p, \psi_p, \tau_p]^T \in \mathbb{R}^{5 \times 1}$ denotes the unknown parameters of the p -th path, and $|g_p|, \angle g_p$ separately represent the amplitude and phase of the complex-valued path gain. Then, for an unbiased estimator, the estimation variance is bounded by CRLB, which is the inverse of the $5P \times 5P$ Fisher information matrix (FIM) $\mathcal{F}(\boldsymbol{\xi})$ [12] defined as

$$[\mathcal{F}(\boldsymbol{\xi})]_{i,j} = \mathbb{E}_{\mathbf{y}|\boldsymbol{\xi}} \left\{ \frac{\partial \ln p(\mathbf{y} | \boldsymbol{\xi})}{\partial \xi_i} \frac{\partial \ln p(\mathbf{y} | \boldsymbol{\xi})}{\partial \xi_j} \right\}, \quad (18)$$

where $p(\mathbf{y} | \boldsymbol{\xi})$ is the likelihood function of \mathbf{y} conditioned on $\boldsymbol{\xi}$, and the expectation is taken over the noise distribution. The $5P \times 5P$ FIM can be sliced into P^2 submatrices as

$$\mathcal{F}(\boldsymbol{\xi}) = \begin{bmatrix} \mathcal{F}(\boldsymbol{\xi}_1, \boldsymbol{\xi}_1) & \cdots & \mathcal{F}(\boldsymbol{\xi}_1, \boldsymbol{\xi}_P) \\ \vdots & \ddots & \vdots \\ \mathcal{F}(\boldsymbol{\xi}_P, \boldsymbol{\xi}_1) & \cdots & \mathcal{F}(\boldsymbol{\xi}_P, \boldsymbol{\xi}_P) \end{bmatrix}, \quad (19)$$

where $\mathcal{F}(\boldsymbol{\xi}_i, \boldsymbol{\xi}_j)$ is a 5×5 matrix. Generally, a closed-form CRLB analysis for multipath channel estimation is hard to obtain [13]. Moreover, if two or more paths have an extremely close angle

and delay, the rank deficiency of $\mathcal{F}(\xi)$ appears, which causes the determinant of $\mathcal{F}(\xi)$ to be close to 0. However, the number of paths to the BS is very small and these paths are characterized by separation in delay in wideband mmWave systems. Hence, we assume that $\mathcal{F}(\xi)$ is nonsingular and can be transformed into a block diagonal matrix [12], and each submatrix on the diagonal of $\mathcal{F}(\xi)$ can be written as

$$\mathcal{F}(\xi_p, \xi_p) = \begin{bmatrix} \mathcal{F}(|g_p| | g_p) & \mathcal{F}(|g_p, \angle g_p) & \mathcal{F}(|g_p, \phi_p) & \mathcal{F}(|g_p, \psi_p) & \mathcal{F}(|g_p, \tau_p) \\ \mathcal{F}(\angle g_p | g_p) & \mathcal{F}(\angle g_p, \angle g_p) & \mathcal{F}(\angle g_p, \phi_p) & \mathcal{F}(\angle g_p, \psi_p) & \mathcal{F}(\angle g_p, \tau_p) \\ \mathcal{F}(\phi_p | g_p) & \mathcal{F}(\phi_p, \angle g_p) & \mathcal{F}(\phi_p, \phi_p) & \mathcal{F}(\phi_p, \psi_p) & \mathcal{F}(\phi_p, \tau_p) \\ \mathcal{F}(\psi_p | g_p) & \mathcal{F}(\psi_p, \angle g_p) & \mathcal{F}(\psi_p, \phi_p) & \mathcal{F}(\psi_p, \psi_p) & \mathcal{F}(\psi_p, \tau_p) \\ \mathcal{F}(\tau_p | g_p) & \mathcal{F}(\tau_p, \angle g_p) & \mathcal{F}(\tau_p, \phi_p) & \mathcal{F}(\tau_p, \psi_p) & \mathcal{F}(\tau_p, \tau_p) \end{bmatrix}. \quad (20)$$

Considering that the inverse of a block diagonal matrix is a block diagonal matrix with the inverse of the original blocks on its diagonal, we can separately calculate the inverse matrix of each submatrix. Thus, $\mathcal{F}(\xi_p, \xi_p)$ can be derived as in Appendix and the FIM $\mathcal{F}(\xi)$ can be obtained.

Let us define the channel statement information (CSI) as

$$\tilde{H}_{k,m,b} = \sum_{p=0}^{P-1} |g_p| e^{j\angle g_p} \check{A}_{k,m,b,p} e^{-j2\pi k \Delta f \tau_p}. \quad (21)$$

From [13], the lower bound of the CSI can be obtained via the transformation vector $\partial \tilde{H}_{k,m,b} / \partial \xi$ as

$$\text{LB}_{k,m,b}(\xi) = \left(\frac{\partial \tilde{H}_{k,m,b}}{\partial \xi} \right)^H \mathcal{F}^{-1}(\xi) \frac{\partial \tilde{H}_{k,m,b}}{\partial \xi}, \quad (22)$$

where the entries of $\partial \tilde{H}_{k,m,b} / \partial \xi$ are given as

$$\begin{aligned} \frac{d\tilde{H}_{k,m,b}}{d|g_p|} &= e^{j\angle g_p} \check{A}_{k,m,b,p} e^{-j2\pi k \Delta f \tau_p}, & \frac{d\tilde{H}_{k,m,b}}{d\angle g_p} &= j|g_p| e^{j\angle g_p} \check{A}_{k,m,b,p} e^{-j2\pi k \Delta f \tau_p}, \\ \frac{d\tilde{H}_{k,m,b}}{d\phi_p} &= |g_p| e^{j\angle g_p} e^{-j2\pi k \Delta f \tau_p} \frac{\partial \check{A}_{k,m,b,p}}{\partial \phi_p}, & \frac{d\tilde{H}_{k,m,b}}{d\psi_p} &= |g_p| e^{j\angle g_p} e^{-j2\pi k \Delta f \tau_p} \frac{\partial \check{A}_{k,m,b,p}}{\partial \psi_p}, \\ \frac{d\tilde{H}_{k,m,b}}{d\tau_p} &= -j2\pi k \Delta f |g_p| e^{j\angle g_p} \check{A}_{k,m,b,p} e^{-j2\pi k \Delta f \tau_p}. \end{aligned} \quad (23)$$

Finally, the CSI error (22) can be constructed by solving the inverse of $\mathcal{F}(\xi)$, where the inversion process of $\mathcal{F}(\xi)$ is omitted due to space limitations.

IV. SIMULATION RESULTS

In this section, we evaluate the performance of the proposed scheme for the wideband channel estimation over RIS assisted mmWave MIMO. The system parameter settings are as follows. The carrier frequency is $f_c = 28$ GHz, the bandwidth is $W = 600$ MHz, and the number of subcarriers is $N_c = 512$. The RIS assisted mmWave channel parameter settings are: the number of antennas at BS is $N_b = 64$, the antenna spacing is $d = \lambda_c/2$, the number of paths is $P = 5$, and τ_p , ϕ_p and ψ_p are uniformly distributed within $[0, 32/W)$, $[-\pi/2, \pi/2)$ and $[-\pi/2, \pi/2)$, respectively. Moreover, during the channel estimation, the under-sampling rates in the greedy searching are set as $\eta_\phi = 2$, $\eta_\psi = 2$ and $\eta_\tau = 2$, the over-sampling rates in the precise searching are set as $\eta_\phi = 4$, $\eta_\psi = 4$ and $\eta_\tau = 4$, and the iteration number of the single refinement and cyclic refinement are set as $R_s = R_c = 5$.

The signal-to-noise ratio (SNR) is expressed as $10 \log_{10} \sigma_t^2 / \sigma_v^2$, where σ_t^2 is the average power of the effective signal. Here, we use the normalized mean square error (NMSE) for the channel parameters as performance metric, which is defined as $\text{NMSE}_{\hat{x}} = \mathbb{E} \left\{ \frac{\|\hat{x} - x\|^2}{\|x\|^2} \right\}$ with \hat{x} being the estimate of x and the p -th element of x consisting of $\{g_p, \phi_p, \psi_p, \tau_p\}$. Note that $\mathbf{g} = [g_0, \dots, g_{P-1}]^T$, $\boldsymbol{\phi} = [\phi_0, \dots, \phi_{P-1}]^T$, $\boldsymbol{\psi} = [\psi_0, \dots, \psi_{P-1}]^T$, $\boldsymbol{\tau} = [\tau_0, \dots, \tau_{P-1}]^T$, and the NMSE of ‘Angle ϕ/ψ ’ in Fig. 2 and Fig. 3 denotes the average of the angle ϕ ’s NMSE and ψ ’s NMSE.

Fig. 2 plots the NMSEs of channel parameters estimates with respect to SNR, where the number of pilot symbols is $M = 5, 10, 15$, respectively. Notice that the number of pilot carriers and elements at RIS are fixed to $L = 12$ and $N_r = 16 \times 16$, respectively. It can be seen from Fig. 2 that all NMSEs decrease as the SNR increases, and the proposed scheme achieves a good estimation performance even at low SNR, which demonstrates its effectiveness. Moreover, for the same SNR, the NMSE decreases with the increase of M , which shows that more pilot symbols can enhance the parameter recovery performance.

Fig. 3 plots the NMSEs of channel parameters estimates versus SNR for different L and N_r , where $M = 16$. It can be seen from Fig. 3 that all NMSEs of the parameters decrease as the SNR increases. At the same SNR, the performance of parameter estimation becomes better as the number of RIS elements or pilot subcarriers increases as expected.

In Fig. 4, we employ the NMSE of estimated cascaded channels, i.e., $\text{NMSE}_{\tilde{\mathbf{H}}} = \mathbb{E} \left\{ \frac{\|\hat{\tilde{\mathbf{H}}} - \tilde{\mathbf{H}}\|^2}{\|\tilde{\mathbf{H}}\|^2} \right\}$, as performance indicator with $\hat{\tilde{H}}_{k,m,b}$ as the estimate of $\tilde{H}_{k,m,b}$, where $\tilde{\mathbf{H}} = [\tilde{H}_{0,0,0}, \dots, \tilde{H}_{L-1,M-1,N_b-1}]^T$. Fig. 4 compares the cascaded channel NMSEs of the OMP method [14], the NOMP method and

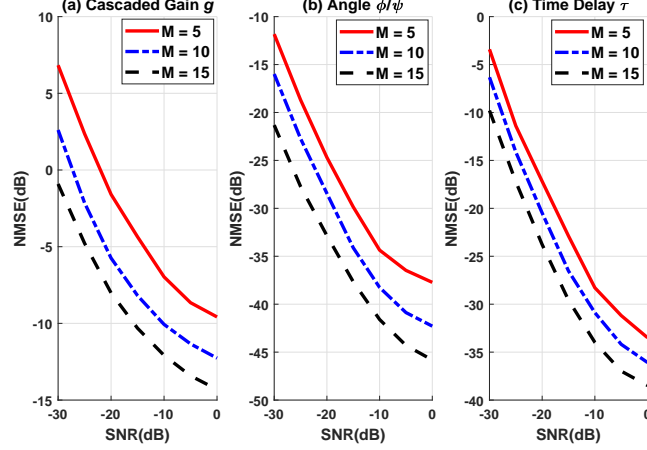


Fig. 2. NMSEs of channel parameters versus SNR at different M .

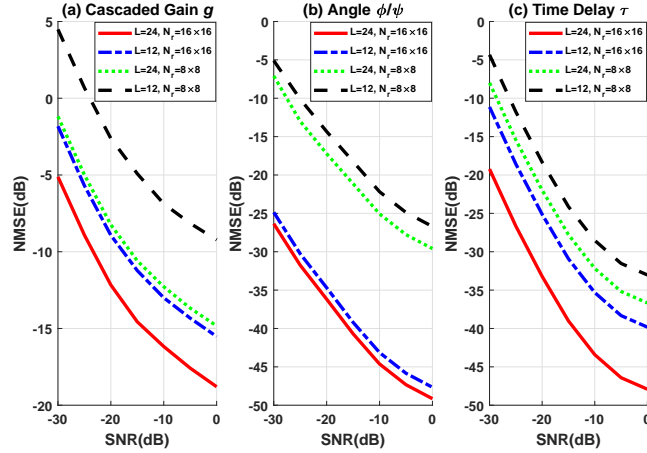


Fig. 3. NMSEs of channel parameters versus SNR at different L and N_r .

CRLB at different SNRs, where $M = 16$, $L = 12$ and $N_r = 16 \times 16$. It can be seen from Fig. 4 that the NMSE of the proposed NOMP method is always better than that of the OMP method, and the gap between the NOMP and OMP methods increases with the SNR increase. Moreover, it can be checked that the performance of the OMP method is limited by the sampling rate of searching and the extended Newton method can further enhance the estimation performance.

V. CONCLUSION

In this letter, we have presented a wideband channel estimation scheme for an RIS assisted mmWave MIMO system. We have firstly described the two individual channels and the frequency

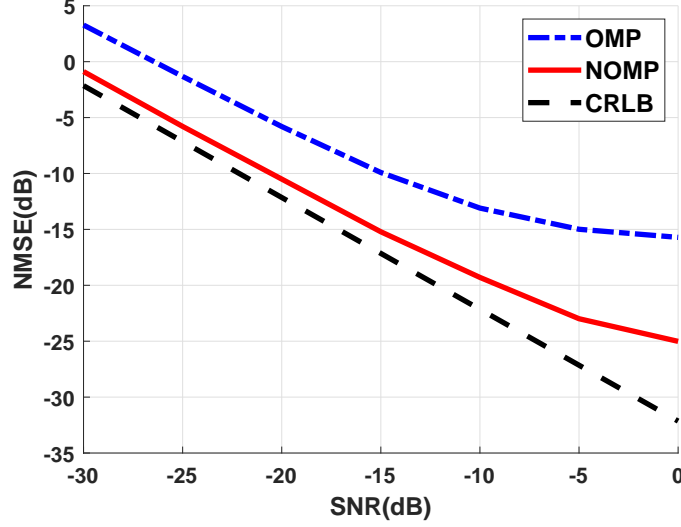


Fig. 4. Comparison of cascaded channels' NMSEs of OMP, NOMP and CRLB versus SNR.

response of the received signal, where the wideband effect is considered. Then, we have expressed channel estimation as a parameter recovery problem and utilized the NOMP algorithm to estimate the channel with a few OFDM pilot symbols. Moreover, we have derived the CRLB for channel estimates. Simulation results have verified that the proposed channel estimation scheme achieves promising NMSE performances, especially at low SNR and with a few pilot symbols.

APPENDIX

From (20), we can derive $\mathcal{F}(\xi_p, \xi_p)$ as

$$\begin{aligned}
 \mathcal{F}(\xi_p, \xi_p) = & \frac{2}{\sigma_v^2} \begin{bmatrix} 1 & |g_p| & |g_p| & |g_p| & 2\pi\Delta f|g_p| \\ |g_p| & |g_p|^2 & |g_p|^2 & |g_p|^2 & 2\pi\Delta f|g_p|^2 \\ |g_p| & |g_p|^2 & |g_p|^2 & |g_p|^2 & 2\pi\Delta f|g_p|^2 \\ |g_p| & |g_p|^2 & |g_p|^2 & |g_p|^2 & 2\pi\Delta f|g_p|^2 \\ 2\pi\Delta f|g_p| & 2\pi\Delta f|g_p|^2 & 2\pi\Delta f|g_p|^2 & 2\pi\Delta f|g_p|^2 & (2\pi\Delta f|g_p|)^2 \end{bmatrix} \\
 & \odot \begin{bmatrix} \Re\{[\mathbf{B}_p]_{11}\} - \Im\{[\mathbf{B}_p]_{11}\} & \Re\{[\mathbf{B}_p]_{12}\} & \Re\{[\mathbf{B}_p]_{13}\} & \Im\{[\tilde{\mathbf{B}}_p]_{11}\} \\ \Im\{[\mathbf{B}_p]_{11}\} & \Re\{[\mathbf{B}_p]_{11}\} & \Im\{[\mathbf{B}_p]_{12}\} & \Im\{[\mathbf{B}_p]_{13}\} - \Re\{[\tilde{\mathbf{B}}_p]_{11}\} \\ \Re\{[\mathbf{B}_p]_{21}\} - \Im\{[\mathbf{B}_p]_{21}\} & \Re\{[\mathbf{B}_p]_{22}\} & \Re\{[\mathbf{B}_p]_{23}\} & \Im\{[\tilde{\mathbf{B}}_p]_{21}\} \\ \Re\{[\mathbf{B}_p]_{31}\} - \Im\{[\mathbf{B}_p]_{31}\} & \Re\{[\mathbf{B}_p]_{32}\} & \Re\{[\mathbf{B}_p]_{33}\} & \Im\{[\tilde{\mathbf{B}}_p]_{31}\} \\ -\Re\{[\tilde{\mathbf{B}}_p]_{11}\} - \Re\{[\tilde{\mathbf{B}}_p]_{11}\} - \Im\{[\tilde{\mathbf{B}}_p]_{12}\} - \Im\{[\tilde{\mathbf{B}}_p]_{13}\} & \Re\{C_p\} \end{bmatrix} \quad (24)
 \end{aligned}$$

where $\check{\mathbf{a}}_{k,m,b} \triangleq [\mathbf{a}_B(k\Delta f, \theta_b)]_b \mathbf{a}_R^T(k\Delta f, \phi_r, \psi_r) \mathbf{\Omega}_m$, $\check{A}_{k,m,b,p} \triangleq \check{\mathbf{a}}_{k,m,b} \mathbf{a}_R(k\Delta f, \phi_p, \psi_p)$, $\mathbf{B}_p \triangleq \sum_{k,m,b} \mathbf{D}_{k,m,b,p}$, $\check{\mathbf{B}}_p \triangleq \sum_{k,m,b} k \mathbf{D}_{k,m,b,p}$, $C_p \triangleq \sum_{k,m,b} k^2 \check{A}_{k,m,b,p}^* \check{A}_{k,m,b,p}$,

$$\mathbf{D}_{k,m,b,p} \triangleq \begin{bmatrix} \check{A}_{k,m,b,p}^* \\ \frac{\partial \check{A}_{k,m,b,p}^*}{\partial \phi_p} \\ \frac{\partial \check{A}_{k,m,b,p}^*}{\partial \psi_p} \end{bmatrix} \begin{bmatrix} \check{A}_{k,m,b,p} & \frac{\partial \check{A}_{k,m,b,p}}{\partial \phi_p} & \frac{\partial \check{A}_{k,m,b,p}}{\partial \psi_p} \end{bmatrix}, \quad (25)$$

$$\begin{bmatrix} \frac{\partial \check{A}_{k,m,b,p}}{\partial \phi_p} \\ \frac{\partial \check{A}_{k,m,b,p}}{\partial \psi_p} \\ \frac{\partial \check{A}_{k,m,b,p}^*}{\partial \phi_p} \\ \frac{\partial \check{A}_{k,m,b,p}^*}{\partial \psi_p} \end{bmatrix} = \begin{bmatrix} -j2\pi(1+\frac{k\Delta f}{f_c})\check{\mathbf{a}}_{k,m,b}(\mathbf{a}_R(k\Delta f, \phi_p, \psi_p) \odot \dot{\boldsymbol{\omega}}_{\phi_p}) \\ -j2\pi(1+\frac{k\Delta f}{f_c})\check{\mathbf{a}}_{k,m,b}(\mathbf{a}_R(k\Delta f, \phi_p, \psi_p) \odot \dot{\boldsymbol{\omega}}_{\psi_p}) \\ j2\pi(1+\frac{k\Delta f}{f_c})\check{\mathbf{a}}_{k,m,b}^*(\mathbf{a}_R^*(k\Delta f, \phi_p, \psi_p) \odot \dot{\boldsymbol{\omega}}_{\phi_p}) \\ j2\pi(1+\frac{k\Delta f}{f_c})\check{\mathbf{a}}_{k,m,b}^*(\mathbf{a}_R^*(k\Delta f, \phi_p, \psi_p) \odot \dot{\boldsymbol{\omega}}_{\psi_p}) \end{bmatrix}, \quad (26)$$

$$\dot{\boldsymbol{\omega}}_{\phi_p} = \left[0, \dots, \frac{d((N_x-1)\cos(\phi_p)\sin(\psi_p) + (N_y-1)\cos(\phi_p)\cos(\psi_p))}{\lambda_c} \right]^T, \quad (27)$$

$$\dot{\boldsymbol{\omega}}_{\psi_p} = \left[0, \dots, \frac{d((N_x-1)\sin(\phi_p)\cos(\psi_p) - (N_y-1)\sin(\phi_p)\sin(\psi_p))}{\lambda_c} \right]^T. \quad (28)$$

REFERENCES

- [1] M. Nemati *et al.*, "RIS-assisted coverage enhancement in millimeter-wave cellular networks," *IEEE Access*, vol. 8, pp. 188171-188185, 2020.
- [2] J. Ma *et al.*, "Sparse Bayesian learning for the time-varying massive MIMO channels: Acquisition and tracking," *IEEE Trans. Commun.*, vol. 67, no. 3, pp. 1925-1938, Mar. 2019.
- [3] E. Basar *et al.*, "Present and future of reconfigurable intelligent surface-empowered communications," *arXiv:2105.00671*, 2021. [Online]. Available: <https://arxiv.org/abs/2105.00671>.
- [4] M. Nemati *et al.*, "Modeling RIS empowered outdoor-to-indoor communication in mmWave cellular networks," *arXiv:2101.00736*, 2021. [Online]. Available: <https://arxiv.org/abs/2101.00736>.
- [5] H. Liu *et al.*, "Matrix-calibration-based cascaded channel estimation for reconfigurable intelligent surface assisted multiuser MIMO," *IEEE J. Sel. Areas Commun.*, vol. 38, no. 11, pp. 2621-2636, Nov. 2020.
- [6] J. He *et al.*, "Channel estimation for RIS-aided mmWave MIMO channels," *arXiv:2002.06453*, 2020. [Online]. Available: <https://arxiv.org/abs/2002.06453>.
- [7] X. Hu *et al.*, "Location information aided multiple intelligent reflecting surface systems," *IEEE Trans. Commun.*, vol. 68, no. 12, pp. 7948-7962, Dec. 2020.
- [8] B. Wang *et al.*, "Beam squint and channel estimation for wideband mmWave massive MIMO-OFDM systems," *IEEE Trans. Signal Process.*, vol. 67, no. 23, pp. 5893-5908, Dec. 2019.
- [9] S. Zhang *et al.*, "Deep learning optimized sparse antenna activation for reconfigurable intelligent surface assisted communication," *arXiv:2009.01607*, 2020. [Online]. Available: <https://arxiv.org/abs/2009.01607>.
- [10] B. Deepak *et al.*, "Channel estimation in reconfigurable intelligent surface assisted mmWave MIMO systems," *arXiv:2011.00900*, 2020. [Online]. Available: <https://arxiv.org/abs/2011.00900>.

- [11] Y. Han *et. al.*, “Efficient downlink channel reconstruction for FDD multi-antenna systems,” *IEEE Trans. Wireless Commun.*, vol. 18, no. 6, pp. 3161-3176, Jun. 2019.
- [12] W. -T. Shih *et. al.*, “Fast antenna and beam switching method for mmWave handsets with hand blockage,” *arXiv:2103.08151*, 2021. [Online]. Available: <https://arxiv.org/abs/2103.08151>.
- [13] D. Fan *et. al.*, “Angle domain channel estimation in hybrid millimeter wave massive MIMO systems,” *IEEE Trans. Wireless Commun.*, vol. 17, no. 12, pp. 8165-8179, Dec. 2018.
- [14] J. Lee *et. al.*, “Channel estimation via orthogonal matching pursuit for hybrid MIMO systems in millimeter wave communications,” *IEEE Trans. Commun.*, vol. 64, no. 6, pp. 2370-2386, Jun. 2016.